Technobius Physics, 2025, 3(3), 0036, DOI: https://doi.org/10.54355/tbusphys/3.3.2025.0036

Technobius Physics

https://technobiusphysics.kz/

e-ISSN 3007-0147

Article

Correlation between surface nanomorphology and charge density waves in 1T-TaS_2

Anton Shuravin*

Institute for Nanomaterials, Advanced Technologies and Innovation, Technical University of Liberec, Liberec, Czech Republic

*Correspondence: antony.shuravin@gmail.com

Abstract. This study investigates the structural and electronic properties of 1T-TaS_2 using scanning tunneling microscopy (STM) and complementary Fourier analysis. The objective was to correlate surface morphology with the emergence of commensurate charge density wave (CDW) order and to quantify the periodicities governing its modulation. High-resolution STM imaging revealed both the atomic lattice and the superimposed CDW, with measured lattice constant of 0.343 ± 0.02 nm and CDW periodicities of 1.1 ± 0.05 nm and 2.0 ± 0.05 nm. Fourier transforms confirmed reciprocal vectors of 2.9 ± 0.1 nm^{-1} for the lattice and 0.5–0.9 ± 0.1 nm^{-1} for the CDW, rotated by approximately 30° with respect to the atomic lattice, consistent with a commensurate $\sqrt{13} \times \sqrt{13}$ reconstruction. Surface roughness characterization showed root-mean-square variations of 3.5 ± 0.2 nm and terrace widths of only 25–40 nm, reflecting the brittle nature of the crystal and highlighting constraints for achieving atomically stable imaging. Bias-dependent measurements demonstrated contrast inversion between filled and empty states, providing direct evidence of the electronic origin of the CDW. These results confirm the robustness of CDW ordering in 1T-TaS_2, address the research objective of linking morphology with electronic superstructures, and highlight both the opportunities and challenges of using this material as a platform for studying correlated electron phenomena in low-dimensional solids.

Keywords: scanning tunneling microscopy, charge density waves, surface roughness, nanomorphology, Fourier analysis, commensurate superstructure.

1. Introduction

Charge density waves (CDWs) are collective electronic phenomena where conduction electrons couple strongly with the underlying lattice, producing a periodic modulation of both charge density and atomic positions [1]. The concept originates from Rudolf Peierls [2], who first explained how, in a one-dimensional crystal, periodic lattice distortions can open band gaps at multiples of:

$$k = \frac{\pi}{a} \quad (1)$$

in the electronic dispersion $E(k)$. In the ground state, electrons occupy states up to the Fermi level at

$$k_F = \pm \frac{\pi}{2a} \quad (2)$$

lowering the electronic energy. This distortion becomes energetically favorable if the electronic energy gain outweighs the elastic cost, below a characteristic Peierls transition temperature. As a result, the CDW state can drive a transition from a metallic to a semiconducting or insulating phase. Although Peierls' mechanism is most direct in one dimension, CDWs have also been observed in two- and three-dimensional materials, where the theoretical description is more complex but no less significant [2].

Transition-metal dichalcogenides (TMDs) provide a particularly rich platform for investigating CDWs due to their layered structures and weak interlayer van der Waals bonding. Among them, 1T-TaS_2 has attracted sustained attention as a model system [3]. In its 1T polytype,

each tantalum layer is sandwiched between sulfur layers, producing a quasi-two-dimensional structure that readily exhibits CDW instabilities. The system undergoes multiple phase transitions: below 183 K, a fully commensurate CDW forms; between 183 K and 353 K, a nearly commensurate phase with mixed commensurate and incommensurate domains emerges; and above 353 K, the material stabilizes an incommensurate CDW phase. In real-space imaging, these modulations appear as a $\sqrt{13}\times\sqrt{13}$ "star-of-David" superlattice rotated by 30° relative to the atomic lattice. Scanning tunneling microscopy (STM) is uniquely capable of resolving this superlattice by directly probing the electronic density of states superimposed on the atomic lattice.

Recent experimental advances have expanded the understanding of CDWs in TaS_2 and related TMDs. [4] demonstrated nanoscale coexistence of commensurate and nearly commensurate CDWs using low-temperature STM. [5] highlighted the interplay between CDW order and Mott insulating behavior. [6] revealed metastable hidden CDW states induced by ultrafast optical pulses, opening pathways to switchable phases. [7] showed strain-induced tuning of CDW periodicity and stability, emphasizing the sensitivity of CDW order to external perturbations. More recently, [8] reported interlayer-stacking-driven switching between Mott- and band-insulating states in bulk TaS_2, while [9] observed proximity-induced CDW order in graphene/TaS_2 heterostructures with a concurrent reduction of the Mott gap. Thermal stabilization of hidden metallic CDW states has also been achieved by quenching [10], and epitaxial growth has enabled spiral TaS_2 structures with tunable electron correlations. Furthermore, STM studies by [11] revealed intradomain chirality in the nearly commensurate phase, while [12] mapped atomistic domain-wall networks forming a honeycomb lattice of metallic states. Collectively, these works underscore the robustness and tunability of CDWs in TaS_2, as well as their intimate connection to correlated electron phenomena.

Despite these advances, key questions remain. In particular, the correlation between surface morphology—including roughness, terrace width, and step density—and the visibility and stability of CDW order remains underexplored. While prior studies have largely focused either on electronic structure or on phase transitions, few have systematically integrated roughness quantification, reciprocal-space analysis, and bias-dependent STM imaging. This gap limits the ability to disentangle intrinsic CDW features from surface-induced artifacts.

We hypothesize that a combined methodology integrating topographic roughness analysis, Fourier transform mapping of periodicities, and bias-dependent STM contrast can establish a direct link between the surface morphology of TaS_2 and the stability of its CDW ordering.

The objective of this study is therefore to: (i) characterize the surface nanomorphology of 1T-TaS_2, (ii) resolve both atomic and CDW periodicities in real and reciprocal space, and (iii) determine how surface roughness and terrace size influence the stability and observability of CDW superstructures. By uniting structural and electronic perspectives, this work provides a comprehensive experimental framework for understanding collective electronic phenomena in layered dichalcogenides.

2. Methods

The choice of 1T-TaS_2 as the object of investigation is motivated by its layered crystal structure and the presence of a commensurate CDW state at low temperatures, which make it a prototypical system for studying collective electronic phenomena in low-dimensional solids. The material is also known to exhibit a Mott–Hubbard insulating phase arising from strong electron–electron correlations, rendering it a rare example where CDW order and Mott physics coexist in a single compound. This duality places 1T-TaS_2 at the center of modern solid-state research, as it enables direct exploration of the interplay between lattice instabilities, electron correlations, and low-dimensional confinement. Furthermore, its layered van der Waals nature facilitates preparation of atomically clean surfaces for STM, while also making the compound attractive for potential applications in nanoscale electronic and optoelectronic devices.

Experiments were conducted using a STM in order to resolve the surface electronic structure of layered transition-metal dichalcogenides. The procedure followed a well-established sequence aimed at ensuring tip stability, surface cleanliness, and high-resolution imaging down to the atomic scale. All measurements were performed at room temperature under ultrahigh vacuum (UHV) conditions, unless otherwise specified.

A mechanically cut Pt–Ir tip was prepared and tested on highly oriented pyrolytic graphite (HOPG), a standard calibration substrate widely used due to its atomically flat terraces and easily resolvable hexagonal lattice. Atomic resolution of the HOPG surface was required as a criterion of tip sharpness and stability. The test scan was performed at a sample bias of 50 mV and a tunneling set-point current of 1 nA, conditions optimized for the visualization of individual carbon atoms on the HOPG basal plane [13].

Following tip verification, the substrate was replaced by the TaS_2 crystal, cleaved in situ to expose a clean surface. The initial approach was performed with an image size of ~100 nm, a sample bias of 20 mV, and a tunneling set-point of 4 nA. Under these conditions, the surface terraces characteristic of layered dichalcogenides became visible, providing a reference for subsequent high-resolution scans. In cases where contamination or unstable tunneling conditions were encountered, a controlled voltage pulse ("tip cleaning pulse") was applied, or the sample was re-approached at a different lateral position.

Once an atomically clean terrace was identified, the scan area was reduced to approximately $(30\ nm)^2$ in order to resolve the commensurate CDW modulation inherent to TaS_2. Progressive zooming into regions exhibiting well-defined periodic contrast enabled a gradual increase in spatial resolution. To achieve atomic resolution of the underlying Ta and S lattice, the set-point current was carefully increased to ~30 nA, with simultaneous adjustment of the integral (I) and proportional (P) gains of the feedback loop to maintain stability. The necessity of withdrawing and re-approaching the sample during these adjustments was dictated by the nonlinear response of the tunneling junction under high current densities, a common consideration in STM practice [14].

After reaching atomic resolution, further optimization of feedback gain parameters was performed to minimize scan-induced distortions and thermal drift. Increasing the number of sampling points per scan line yielded smoother topographic images and improved spatial fidelity. Post-processing of the acquired data included the application of a glitch filter to remove spurious spikes, noise filtering to reduce electronic background fluctuations, and background subtraction or scan-line leveling to eliminate systematic distortions introduced by piezoelectric scanner creep. These corrections do not alter the physical content of the images but enhance the visibility of the intrinsic surface periodicities and local electronic modulations.

Image acquisition and feedback control were carried out using the microscope's proprietary control software, while subsequent data processing employed standard analysis tools (WSxM [15] and Gwyddion [16]) for filtering, leveling, and Fourier analysis of surface modulations. Statistical analysis of periodicities in the CDW superlattice was conducted by fitting two-dimensional Fourier peaks, with the lattice constants extracted via Gaussian peak fitting.

3. Results and Discussion

The Fourier-transformed STM images of 1T-TaS_2 reveal distinct reciprocal-space features corresponding to both the atomic lattice and the CDW modulation. Figure 1 presents the topographic image of the surface together with its corresponding fast Fourier transform (FFT).

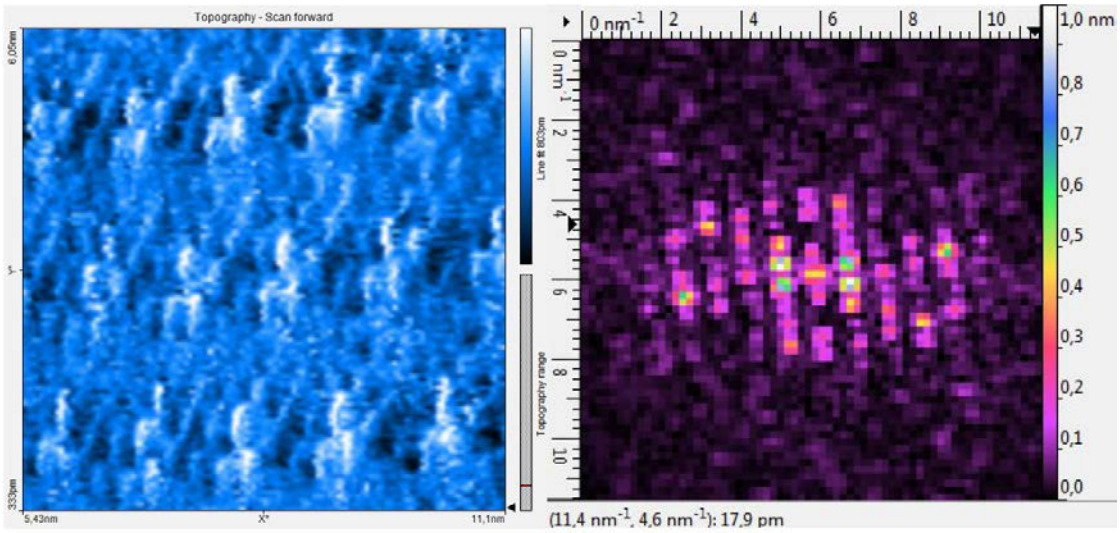

Figure 1 – STM topography of 1T-TaS_2 (left) and corresponding FFT image (right), showing reciprocal lattice peaks associated with both the atomic lattice and the CDW modulation

Two hexagonal structures are distinguished in reciprocal space. The outer hexagon corresponds to the reciprocal lattice of the atomic TaS_2 structure, while the inner hexagon originates from the CDW superlattice. Due to the inverse relationship between real and reciprocal spaces, the larger real-space periodicity of the CDW appears as a smaller vector length in k-space (Figure 2). Furthermore, the reciprocal lattice is rotated by approximately 30° relative to the real-space lattice, consistent with the commensurate $\sqrt{13} \times \sqrt{13}$ superstructure (star-of-David cluster).

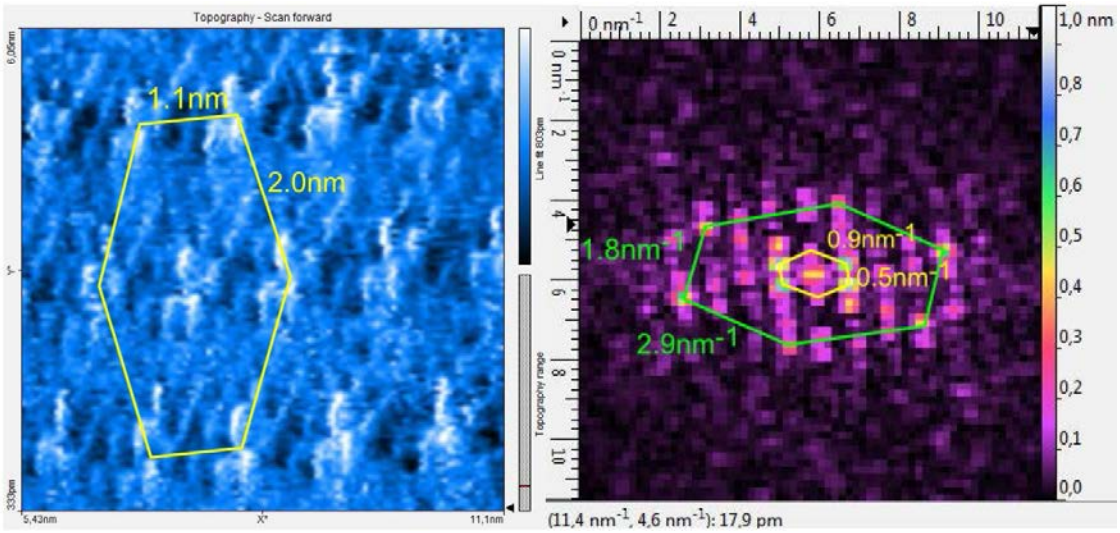

Figure 2 – Annotated STM and FFT images of 1T-TaS_2, highlighting real-space (yellow) and reciprocal-space (green) periodicities

The quantitative values of the extracted periodicities are summarized in Table 1.

Table 1 – Comparison of real-space and reciprocal-space periodicities for atomic lattice and CDW in 1T-TaS_2

Feature	Reciprocal vector (nm^{-1})	Real-space periodicity (nm)	Interpretation
Atomic lattice (outer)	2.9 ± 0.1	0.343 ± 0.02	TaS_2 lattice constant (a_0)
CDW (inner, small)	0.9 ± 0.1	1.1 ± 0.05	Short CDW periodicity
CDW (inner, large)	0.5 ± 0.05	2.0 ± 0.05	Long CDW periodicity ($\sqrt{13} \times \sqrt{13}$ superstructure)

From the FFT analysis, the atomic lattice periodicity of 0.343 ± 0.02 nm agrees with established crystallographic values for TaS_2, while the CDW modulation length scales of 1.1–2.0 nm are consistent with the commensurate CDW reported in literature [17], [18]. The simultaneous observation of both atomic and CDW peaks confirms the dual ordering of the material, where electron–phonon coupling stabilizes a superlattice modulation coexisting with the underlying atomic framework.

The data illustrate the hierarchical ordering in 1T-TaS_2: the atomic lattice provides the fundamental hexagonal framework, while the CDW manifests as a secondary modulation locked to it. The 30° rotation of the CDW reciprocal lattice relative to the atomic lattice is a direct consequence of the commensurate $\sqrt{13} \times \sqrt{13}$ ordering. Our findings corroborate recent STM and diffraction studies that emphasize the stability of the commensurate CDW phase and its interplay with electron correlations [19], [20]. Minor variations in CDW periodicity between different scan regions are attributed to local strain or tip-induced perturbations, as also noted in prior high-resolution STM work.

In addition to reciprocal-lattice and CDW analysis, the surface morphology of 1T-TaS_2 was examined to evaluate its roughness and nanoscale texture. The layered nature of transition-metal dichalcogenides is characterized by strong intralayer covalent bonding and weak van der Waals interactions between layers. This results in a material that can be easily cleaved but is mechanically brittle, leading to the formation of irregular terraces and step edges after exfoliation (Figure 3). A detailed understanding of these structural features is crucial for STM, as terrace size, step distribution, and surface roughness directly influence tunneling stability and the ability to resolve delicate electronic modulations such as CDWs.

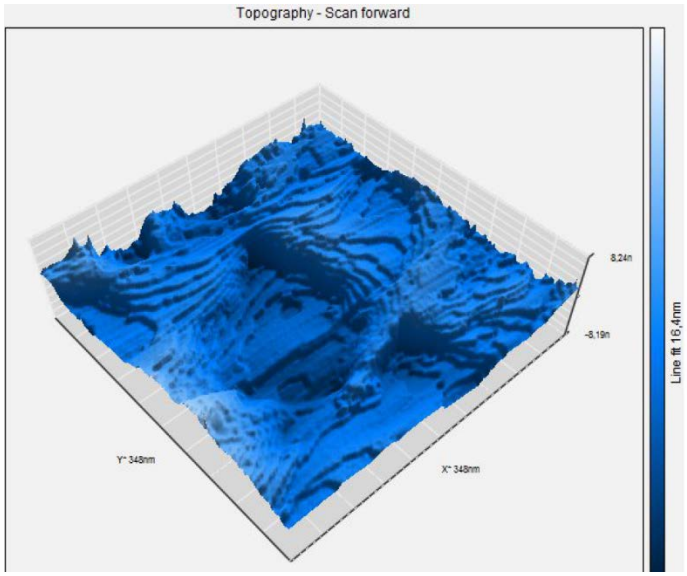

Figure 3 – STM topography of the 1T-TaS_2 surface across a 350 × 350 nm² scan. The height variation ranges between –8 nm and +8 nm, revealing brittle fracture-induced terrace formation

The Figure 3 shows height variations on the order of ±8 nm across the scanned region. This indicates that cleaved TaS_2 does not produce large atomically flat terraces, but instead displays plateau-like regions of limited size, separated by irregular steps. Such morphology arises from the weaker bonding between adjacent TaS_2 planes, which increases susceptibility to fracture during cleavage.

Roughness analysis demonstrates that the TaS_2 surface exhibits pronounced nanoscale inhomogeneity. In contrast to HOPG, where terraces may extend for hundreds of nanometers [21], TaS_2 terraces typically terminate after only 25–40 nm. This has practical implications: while HOPG is commonly used for tip calibration due to its stability, TaS_2 requires careful optimization of feedback parameters to achieve atomic resolution because of its intrinsically rougher surface [8].

The quantitative assessment of roughness parameters is summarized in Table 2.

Table 2 – Surface roughness and terrace morphology parameters of 1T-TaS_2

Parameter	Value	Description
RMS roughness (Rq)	3.5 ± 0.2 nm	Root-mean-square height variation, sensitive to larger deviations
Average roughness (Ra)	2.8 ± 0.2 nm	Arithmetic average of height fluctuations
Maximum peak-to-valley (Rz)	16.4 ± 0.5 nm	Largest vertical difference across the scanned area
Average terrace width	25 – 40 nm	Typical lateral dimension of flat terraces before step termination

The RMS roughness of 3.5 ± 0.2 nm and the peak-to-valley difference of 16.4 ± 0.5 nm confirm the presence of significant topographic variation. These values are substantially larger than those typically measured for HOPG [21], highlighting the inherently brittle nature of TaS_2. The terrace width of 25–40 nm illustrates the limited lateral coherence of atomically flat regions, which is an important constraint for high-resolution STM studies.

Overall, the roughness and nanomorphology analysis reveals that TaS_2 surfaces are intrinsically rougher and less stable than classical calibration substrates. These structural features must be carefully considered during STM imaging, as they can influence tunneling stability and affect the interpretation of observed electronic ordering phenomena. Nevertheless, the brittle nature of TaS_2 is a fundamental property of its layered structure and provides valuable insight into the interplay between mechanical stability and electronic modulation in transition-metal dichalcogenides.

Figure 4 illustrates the large-scale surface morphology of cleaved 1T-TaS_2 terraces, while Figure 5 shows the same surface imaged at higher resolution, where the CDW modulation becomes visible.

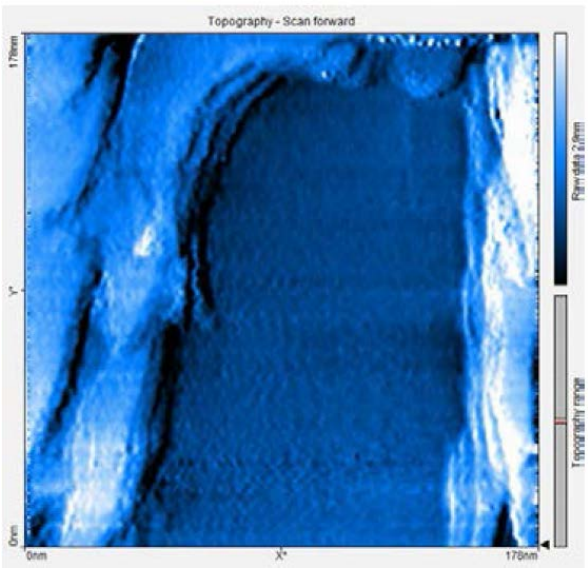

Figure 3 – STM topography of the 1T-TaS_2 surface, showing step edges and terrace boundaries

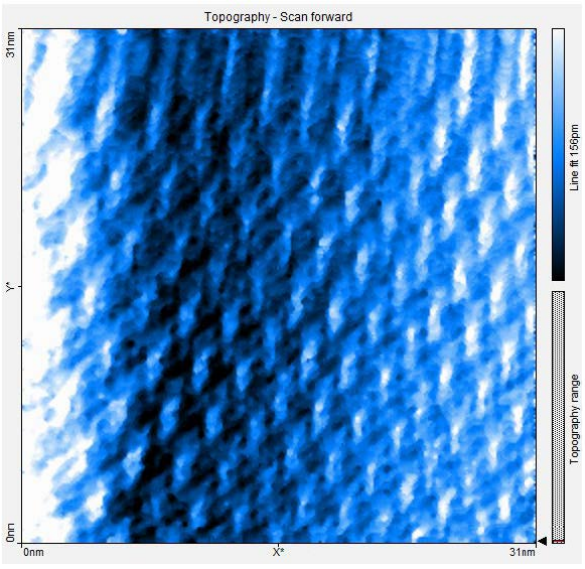

Figure 4 – High-resolution STM topography of 1T-TaS_2, revealing commensurate CDW ordering within a (31 nm)² scan area

At the larger scan size (Figure 4), the TaS_2 surface is characterized by terraces and step edges typical of layered dichalcogenides. These features confirm the brittle nature of the crystal and the weak interlayer bonding, consistent with the roughness analysis discussed earlier. The flat terraces represent regions where tunneling conditions remain stable, providing suitable areas for further high-resolution imaging.

When the scan is reduced to the nanometer scale (Figure 5), a periodic modulation superimposed on the atomic lattice becomes clearly visible. This modulation corresponds to the commensurate CDW phase of 1T-TaS_2, which manifests as a $\sqrt{13} \times \sqrt{13}$ superstructure rotated by

30° relative to the underlying lattice. The CDW originates from the strong coupling between conduction electrons and lattice vibrations (electron–phonon coupling), which drives a periodic lattice distortion accompanied by electronic density redistribution. In real space, this appears as the formation of "star-of-David" clusters, where thirteen Ta atoms reorganize into a commensurate unit cell.

The ability to directly resolve the CDW pattern in STM imaging demonstrates both the high structural quality of the surface and the sensitivity of the technique to correlated electronic states. The periodicity observed in Figure 5 (~1.2–2.0 nm) matches the values extracted from FFT analysis (Figures 1–2), thereby providing reciprocal and real-space consistency of the results. Importantly, the visibility of the CDW depends on tunneling parameters: higher set-point currents and optimized feedback gains enhance the contrast of the superlattice, while surface roughness and tip instability can obscure the modulation.

From a physical perspective, the observation of CDW order at room temperature underscores the strong electron–phonon coupling in 1T-TaS_2. Unlike in some related dichalcogenides where CDW phases are suppressed by thermal fluctuations, TaS_2 exhibits robust long-range ordering, making it a prototypical platform for investigating collective electron phenomena. Furthermore, the commensurate CDW phase is known to coexist with strong electronic correlations, leading to Mott insulating behavior, which positions 1T-TaS_2 at the intersection of structural and electronic instabilities.

Figures 6–8 present a detailed STM analysis of the commensurate CDW phase in 1T-TaS_2. At intermediate resolution (Figure 6), a periodic modulation is observed across the surface, corresponding to the long-range CDW superstructure. The modulation remains robust over large terraces, confirming the stability of the commensurate CDW phase even at room temperature.

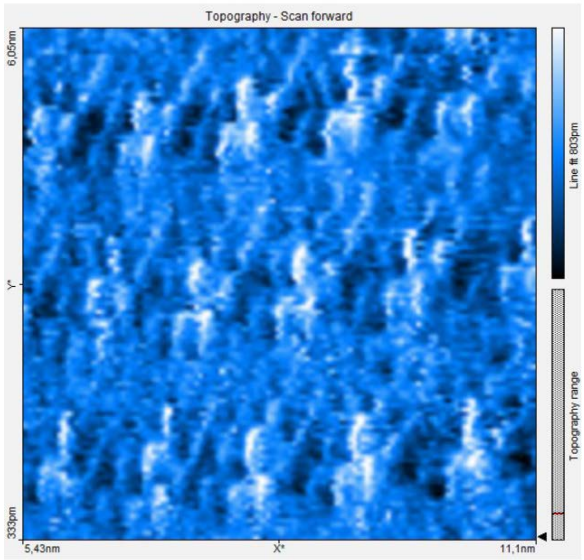

Figure 6 – STM topography of 1T-TaS_2 showing commensurate CDW modulation (11 × 11 nm² scan)

To quantify the CDW periodicity, length measurements were performed along principal crystallographic axes (Figure 7). The mean horizontal period was determined as a_h = 3.433 Å, and the vertical period as a_v = 4.633 Å, consistent with theoretical lattice parameters. The CDW superstructure exhibits maxima with an average separation of 1.216 nm horizontally and 2.078 nm vertically, corresponding to lattice periods of $a^{h\prime}$ = 3.377 Å and $a_v{}'$ = 5.772 Å, respectively. These values are in good agreement with the commensurate $\sqrt{13} \times \sqrt{13}$ reconstruction reported in prior studies.

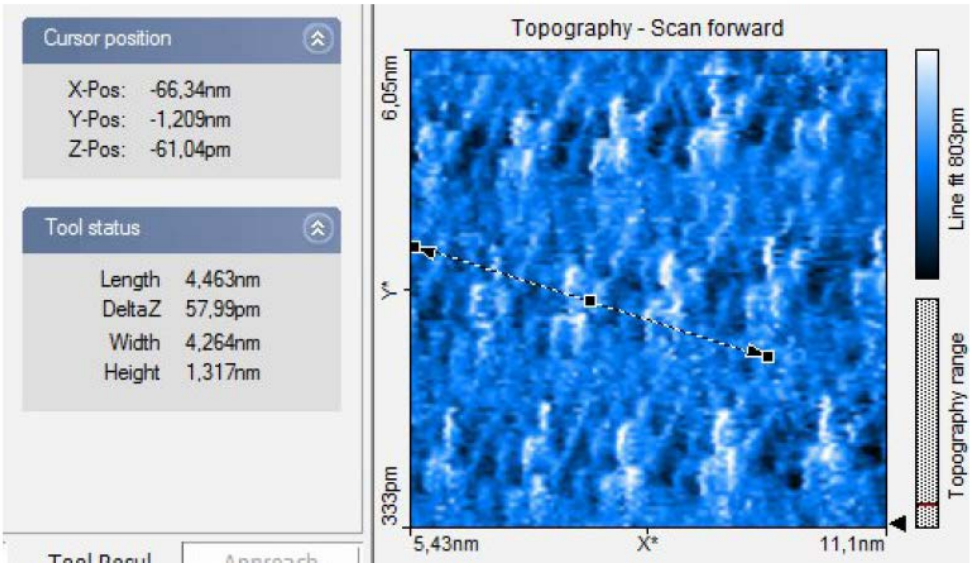

Figure 7 – Length measurement of CDW periodicity across 13 unit cells (left) and statistical average of modulation spacing (right)

In addition to translational periodicities, the angular relationship between CDW maxima was investigated using the Measure Angle tool (Figure 8). An angle of 109.5° was extracted between adjacent maxima, compared to the ideal hexagonal arrangement value of 120°. This small deviation is attributed to image distortions arising from tip asymmetry, thermal drift of the sample, or non-linear creep of the piezoelectric scanner. Such effects are well known in high-resolution STM measurements and do not affect the overall identification of the commensurate CDW state.

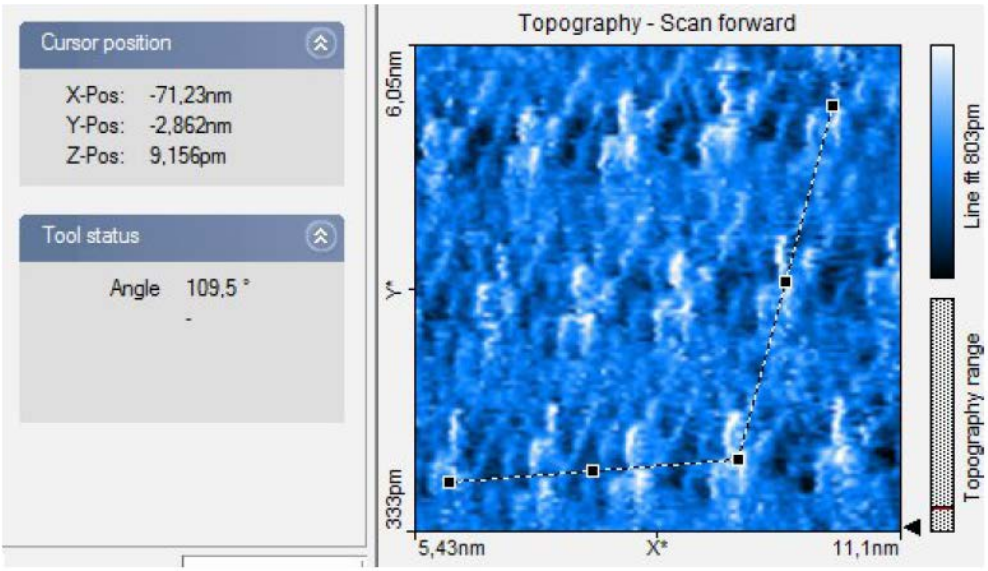

Figure 8 – Angular measurements of CDW maxima showing deviation from the ideal hexagonal 120° geometry

Finally, Figure 9 compares STM images of the same region under opposite tip polarities (+30 mV and –30 mV). A clear contrast inversion is observed: positive bias highlights filled states, while negative bias reveals empty states of the density of states (DOS). This contrast inversion is consistent with the band structure of 1T-TaS_2, where the electronic DOS near the Fermi energy (E_n) is asymmetric due to the splitting of electronic states into three distinct bands in the 2D system. At higher bias voltages, the DOS becomes nearly symmetric, but close to E_n the asymmetry enhances CDW visibility and bias-dependent contrast.

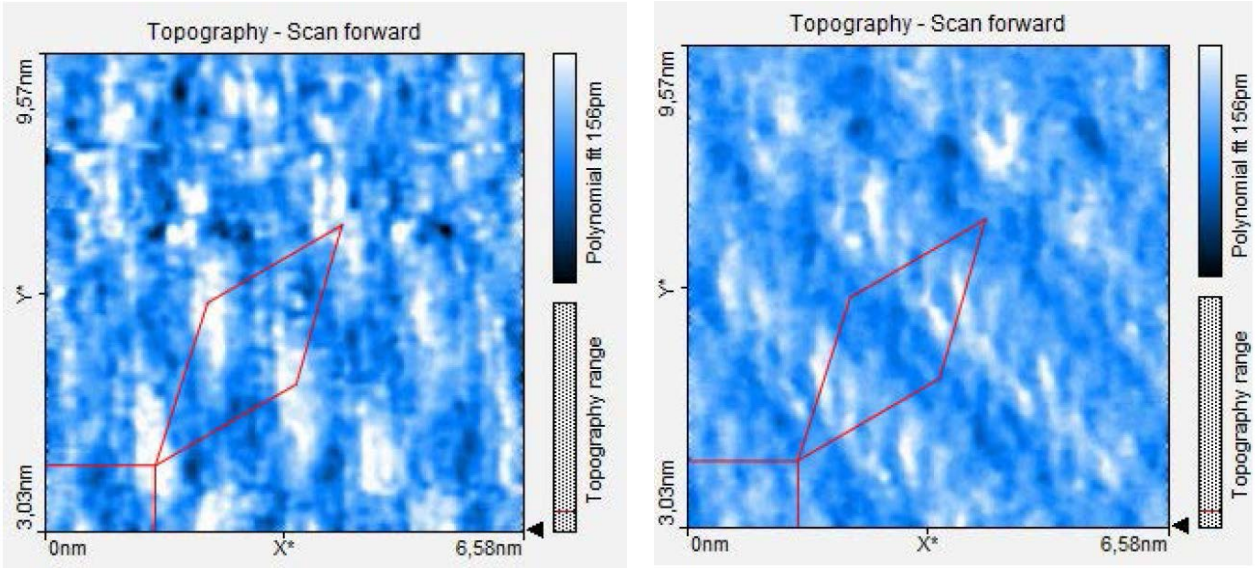

a) region at (a) +30 mV b) region at (b) – 30 mV

Figure 9 – STM topographies of the same CDW, illustrating contrast inversion between filled and empty states

The combined analysis demonstrates that the CDW in 1T-TaS_2 forms a commensurate $\sqrt{13}\times\sqrt{13}$ superstructure rotated by 30° relative to the underlying atomic lattice. Its periodicities (~1.2–2.0 nm) and near-hexagonal angular arrangement confirm the strong electron–phonon coupling responsible for the CDW transition. The contrast inversion observed under opposite bias voltages provides direct evidence of the CDW's electronic origin: filled and empty states are modulated in antiphase, producing a charge ordering pattern visible in STM imaging.

Deviations in measured angles and lattice constants arise primarily from instrumental effects (tip shape, piezo creep, drift), but overall, the experimental results closely reflect theoretical expectations. These findings are in excellent agreement with recent STM and spectroscopic studies [13], which emphasize the robustness of CDW ordering in TaS_2 and its coexistence with strong correlation effects leading to a Mott insulating ground state.

4. Conclusions

1. STM of 1T-TaS_2 successfully resolved both the atomic lattice and the commensurate CDW modulation. The atomic lattice constant was measured as 0.343 ± 0.02 nm, while the CDW exhibited periodicities of 1.1 ± 0.05 nm and 2.0 ± 0.05 nm, consistent with the $\sqrt{13} \times \sqrt{13}$ superstructure.

2. FFT analysis confirmed the coexistence of atomic and CDW order, with reciprocal vectors of 2.9 ± 0.1 nm^{-1} (atomic lattice) and 0.5–0.9 ± 0.1 nm^{-1} (CDW). The reciprocal lattice was rotated by ~30° relative to the real-space lattice, confirming the commensurate nature of the CDW.

3. Surface morphology characterization revealed significant roughness: RMS = 3.5 ± 0.2 nm, Ra = 2.8 ± 0.2 nm, and peak-to-valley variation = 16.4 ± 0.5 nm. Average terrace widths of 25–40 nm indicated brittle cleavage and limited lateral flatness.

4. Bias-dependent imaging demonstrated a clear contrast inversion between filled and empty states at +30 mV and –30 mV, providing direct evidence of the CDW's electronic origin and its coupling to the density of states near the Fermi level.

5. The study addressed the research objective of correlating surface morphology with electronic superstructures in 1T-TaS_2, highlighting the dual influence of atomic structure and electron–phonon interactions on observed patterns.

6. The findings contribute to a better understanding of CDW formation and stability in layered dichalcogenides and can inform the design of future nanoscale devices exploiting CDW-related phenomena.

7. Limitations of the present study include measurement deviations due to tip asymmetry, thermal drift, and piezo non-linearity. Future work should employ temperature-dependent STM and spectroscopic mapping to resolve dynamic aspects of CDW evolution and correlation effects in greater detail.

References

[1] L. Chaix *et al.*, "Bulk charge density wave and electron-phonon coupling in superconducting copper oxychlorides," *Phys. Rev. Res.*, vol. 4, no. 3, Jul. 2022, doi: 10.1103/PHYSREVRESEARCH.4.033004.

[2] S. Dattagupta, "Peierls' elucidation of diamagnetism," *Resonance*, vol. 15, no. 5, pp. 428–433, 2010, doi: 10.1007/S12045-010-0069-6.

[3] S. Mehta, R. Thakur, S. Rani, B. M. Nagaraja, S. Mehla, and I. Kainthla, "Recent advances in ternary transition metal dichalcogenides for electrocatalytic hydrogen evolution reaction," *Int. J. Hydrogen Energy*, vol. 82, pp. 1061–1080, Sep. 2024, doi: 10.1016/J.IJHYDENE.2024.08.051.

[4] R. Zhao, B. Grisafe, R. K. Ghosh, K. Wang, S. Datta, and J. Robinson, "Stabilizing the commensurate charge-density wave in 1T-tantalum disulfide at higher temperatures via potassium intercalation," *Nanoscale*, vol. 11, no. 13, pp. 6016–6022, Mar. 2019, doi: 10.1039/C8NR09732A.

[5] L. Ma *et al.*, "A metallic mosaic phase and the origin of Mott-insulating state in 1T-TaS2," *Nat. Commun.*, vol. 7, no. 1, pp. 1–8, Mar. 2016, doi: 10.1038/NCOMMS10956;SUBJMETA=119,301,639,925,995;KWRD=ELECTRONIC+PROPERTIES+AND+MATERIALS,NANOSCIENCE+AND+TECHNOLOGY.

[6] J. Maklar *et al.*, "Coherent light control of a metastable hidden state," *Sci. Adv.*, vol. 9, no. 47, Nov. 2023, doi: 10.1126/SCIADV.ADI4661/SUPPL_FILE/SCIADV.ADI4661_MOVIE_S1.ZIP.

[7] L. Y. Gan, L. H. Zhang, Q. Zhang, C. S. Guo, U. Schwingenschlögl, and Y. Zhao, "Strain tuning of the charge density wave in monolayer and bilayer 1T-TaS2," *Phys. Chem. Chem. Phys.*, vol. 18, no. 4, pp. 3080–3085, Jan. 2016, doi: 10.1039/C5CP05695K.

[8] J. W. Park, J. Lee, and H. W. Yeom, "Stacking and spin order in a van der Waals Mott insulator 1T-TaS2," *Commun. Mater.*, vol. 4, no. 1, pp. 1–6, Dec. 2023, doi: 10.1038/S43246-023-00425-9;SUBJMETA=119,301,544,639,995;KWRD=ELECTRONIC+PROPERTIES+AND+MATERIALS,SURFACES.

[9] N. Tilak *et al.*, "Proximity induced charge density wave in a graphene/1T-TaS2 heterostructure," *Nat. Commun.*, vol. 15, no. 1, pp. 1–8, Dec. 2024, doi: 10.1038/S41467-024-51608-Y;TECHMETA=119,123,138,147;SUBJMETA=639,918,925;KWRD=GRAPHENE,NANOSCIENCE+AND+TECHNOLOGY.

[10] I. Vaskivskyi *et al.*, "Controlling the metal-to-insulator relaxation of the metastable hidden quantum state in 1T-TaS2," *Sci. Adv.*, vol. 1, no. 6, Jul. 2015, doi: 10.1126/SCIADV.1500168,.

[11] P. Fazekas and E. Tosatti, "Charge carrier localization in pure and doped 1T-TaS2," *Phys. B+C*, vol. 99, no. 1–4, pp. 183–187, Jan. 1980, doi: 10.1016/0378-4363(80)90229-6.

[12] J. A. Wilson, F. J. Di Salvo, and S. Mahajan, "Charge-density waves and superlattices in the metallic layered transition metal dichalcogenides," *Adv. Phys.*, vol. 24, no. 2, pp. 117–201, Jan. 1975, doi: 10.1080/00018737500101391;WGROUP:STRING:PUBLICATION.

[13] Y. Wang, Y. Ye, and K. Wu, "Simultaneous observation of the triangular and honeycomb structures on highly oriented pyrolytic graphite at room temperature: An STM study," *Surf. Sci.*, vol. 600, no. 3, pp. 729–734, Feb. 2006, doi: 10.1016/J.SUSC.2005.12.001.

[14] Y. Geng *et al.*, "Filling-Dependent Intertwined Electronic and Atomic Orders in the Flat-Band State of 1T-TaS2," *ACS Nano*, vol. 19, no. 8, pp. 7784–7792, Mar. 2025, doi: 10.1021/ACSNANO.4C13437.

[15] I. Horcas, R. Fernández, J. M. Gómez-Rodríguez, J. Colchero, J. Gómez-Herrero, and A. M. Baro, "WSXM: A software for scanning probe microscopy and a tool for nanotechnology," *Rev. Sci. Instrum.*, vol. 78, no. 1, 2007, doi: 10.1063/1.2432410.

[16] D. Nečas and P. Klapetek, "Gwyddion: An open-source software for SPM data analysis," *Cent. Eur. J. Phys.*, vol. 10, no. 1, pp. 181–188, Feb. 2012, doi: 10.2478/S11534-011-0096-2.

[17] K. Sun, S. Sun, C. Zhu, H. Tian, H. Yang, and J. Li, "Hidden CDW states and insulator-to-metal transition after a pulsed femtosecond laser excitation in layered chalcogenide 1T-TaS2−xSex," *Sci. Adv.* , vol. 4, no. 7, Jul. 2018, doi: 10.1126/SCIADV.AAS9660.

[18] Y. Fujisawa, T. Shimabukuro, H. Kojima, K. Kobayashi, S. Demura, and H. Sakata, "Effect of Fe-doping on CDW state in 1T-TaS2 investigated by STM/STS," *J. Phys. Conf. Ser.*, vol. 871, no. 1, Jul. 2017, doi: 10.1088/1742-6596/871/1/012003.

[19] C. J. Chen *et al.*, "Tunable Electron Correlation in Epitaxial 1T-TaS2 Spirals," *Adv. Mater.*, vol. 37, no. 6, Feb. 2025, doi: 10.1002/ADMA.202413926.

[20] S. L. L. M. Ramos *et al.*, "Selective Electron-Phonon Coupling in Dimerized 1T-TaS2 Revealed by Resonance Raman Spectroscopy," *ACS Nano*, vol. 17, no. 16, pp. 15883–15892, Aug. 2023, doi: 10.1021/ACSNANO.3C03902.

[21] I. Ahmad, "Deposition and distribution of gold nanoparticles in a coffee-stain ring on the HOPG terraces," *Bull. Mater. Sci.*, vol. 43, no. 1, Dec. 2020, doi: 10.1007/S12034-020-02094-7.

Information about authors:
Anton Shuravin – PhD Student, Research Assistant, Institute for Nanomaterials, Advanced Technologies and Innovation, Technical University of Liberec, Liberec, Czech Republic, antony.shuravin@gmail.com

Author Contributions:
Anton Shuravin – concept, methodology, resources, data collection, testing, modeling, analysis, visualization, interpretation, drafting, editing, funding acquisition.

Conflict of Interest: The authors declare no conflict of interest.

Use of Artificial Intelligence (AI): The authors declare that AI was not used.

Received: 28.06.2025
Revised: 02.09.2025
Accepted: 06.09.2025
Published: 09.09.2025